Floquet Control of Optomechanical Bistability in Multimode Systems

Karl Pelka,[1,*] Guilhem Madiot,[2,†] Rémy Braive,[2,3,4] and André Xuereb[1]
[1]Department of Physics, University of Malta, Msida MSD 2080, Malta
[2]Centre de Nanosciences et de Nanotechnologies, CNRS, Université Paris-Saclay, F-91120 Palaiseau, France
[3]Université de Paris, F-75006 Paris, France
[4]Institut Universitaire de France, F-75231 Paris, France

(Received 1 July 2021; revised 25 April 2022; accepted 19 July 2022; published 14 September 2022)

Cavity optomechanical systems make possible the fine manipulation of mechanical degrees of freedom with light, adding functionality and having broad appeal in photonic technologies. We show that distinct mechanical modes can be exploited with a temporally modulated Floquet drive to steer between distinct steady states induced by changes of cavity radiation pressure. We investigate the additional influence of the thermo-optic nonlinearity on these dynamics and find that it can suppress or amplify the control mechanism in contrast to its often performance-limiting character. Our results provide new techniques for the characterization of thermal properties of optomechanical systems and their control, sensing and computational applications.

DOI: 10.1103/PhysRevLett.129.123603

Introduction.—Cavity optomechanics employs optical forces to exert control over optical fields and mechanical motion in mechanical systems and is a rapidly growing research field with much recent progress [1]. Prototypically, an optomechanical system consists of a single mode of the electromagnetic radiation field, e.g., within a high-finesse optical cavity [2], interacting with the motion of a harmonic oscillator by means of the radiation pressure force [3]. The optomechanical interaction has been used to cool the motion of the mechanical system down to its ground state [4,5] and generate quantum entanglement between mechanical oscillators [6,7]. Through this same interaction, it is also possible to transfer energy from the optical field into the mechanical oscillator; this leads to self-sustained oscillations and lies at the heart of synchronization phenomena in optomechanics [8–18].

Such systems may also find technological use; synchronized optomechanical arrays, for example, could act as on-chip frequency sources [15]. Moreover, mechanical frequency combs [19], proof-of-concept isolators and directional amplifiers for microwave radiation [20–23], and bidirectional conversion between microwave and optical light [24] have all been shown. Control of the optomechanical bistability [25,26] holds technological potential as it provides the means to put mechanical elements controllably into distinct mechanical states. Bistable systems based on optomechanical [27,28] or other [29–31] nonlinearities can act as memory cells for nanomechanical computing, and recently attracted attention in experimental demonstrations of dissipative phase transitions [32,33]. Control over the optomechanical bistability beyond that provided by a uniform drive is of fundamental use as the latter sets limits to the achievable entanglement [34] and enhanced coupling strengths [35].

The study of time-varying optical driving in optomechanics is well established [36] and gained momentum driven by theoretical advances in the Floquet approach [37,38]. It enables nonreciprocal transfer of phonons [39], leading to topological transport of phonons via synthetic gauge fields [40–42], allows quantum states to be transferred from one mechanical element to another [43], and entanglement between such elements [6]. Further studies investigated effects on quantum mechanical properties of mechanical motion [44] and the characterization of the cavity's thermal properties exploiting Floquet techniques [45–48]. Floquet driving has recently proven to overcome mode-competition resulting in mode-locked lasing of nondegenerate modes [49].

In this Letter, we extend the spectral mean field Floquet method underlying [49] enabling its use in Kerr-like models beyond optomechanics [50–52] and incorporating thermo-optical effects. We find that these effects can influence the sideband structure of the optical output spectrum which we demonstrate experimentally. Crucially, our analysis shows that Floquet techniques enable dynamical control of the optomechanical bistability in multimode settings. This presents a useful tool in the manipulation of optomechanical systems, paving the way toward frequency sensing, phononic memory, and logic element applications. Finally, our analysis suggests that thermo-optical nonlinearities can suppress or amplify this novel mechanism, proving that thermal effects can counterintuitively amplify the mechanism.

Model.—We consider the collective dynamics of a system consisting of N mechanical modes coupled to one optical mode, described by the optomechanical Hamiltonian

$$\hat{H}_S/\hbar = \omega_{\mathrm{op}}\hat{a}^\dagger\hat{a} + \sum_{j=1}^{N}[\Omega_j\hat{b}_j^\dagger\hat{b}_j - g_j\hat{a}^\dagger\hat{a}(\hat{b}_j + \hat{b}_j^\dagger)], \quad (1)$$

with $\hat{a}$ ($\hat{b}_j$) being the optical (jth mechanical) annihilation operator, ω_{op} (Ω_j) the corresponding resonance frequencies, and g_j the vacuum optomechanical coupling rates. Extending the Hamiltonian with $i\hbar[\mathcal{E}_{\mathrm{drive}}(t)\hat{a}^\dagger - \mathcal{E}^*_{\mathrm{drive}}(t)\hat{a}]$ includes laser driving. We assume the driving laser $\mathcal{E}_{\mathrm{in}} = \mathcal{E}_0 e^{i\omega_L t}$ to be subjected to optical modulation $\mathcal{E}_{\mathrm{drive}}(t) = \mathcal{E}_{\mathrm{in}}(t)\mathcal{T}(t)$ with a Mach-Zehnder modulator (MZM). Its transfer characteristic $\mathcal{T}(t) = e^{i\phi_0}(1 + e^{i\phi_{\mathrm{mod}}(t)})/2$ realizes intensity modulation, considered throughout this work, expressible as

$$\frac{\mathcal{T}(t)}{e^{i\phi_0}} = \frac{1 - i\mathcal{J}_0(d)}{2} + \sum_{n=1}^{\infty} i^{n+1}\mathcal{J}_n(d)\cos[n\theta(t)] \quad (2)$$

for $\phi_{\mathrm{mod}}(t) = -\pi/2 + d\cos[\theta(t)]$ with $\theta(t) = \Omega_{\mathrm{mod}}t + \theta_0$ and Bessel functions of the first kind $\mathcal{J}_n(d)$. An increasing modulation depth d therefore involves increasingly many driving tones beyond the usual first pair [44–48].

The quantum Langevin equations that describe the open system dynamics [1] are separable into mean-field and fluctuation components $[\hat{a}(t)e^{i\omega_L t + i\phi_0} = \alpha(t) + \hat{\mathfrak{a}}(t)$ and $\hat{b}_j(t) = \beta_j(t) + \hat{\mathfrak{b}}_j(t)]$. The resulting mean-field dynamics with the detuning of the central laser frequency from the optical resonance $\Delta = \omega_{\mathrm{op}} - \omega_L$ and defining $R(z) = z + z^*$ are

$$\dot{\alpha} = \left\{-i\left[\Delta - \sum_{j=1}^{N} g_j R(\beta_j)\right] - \frac{\kappa}{2}\right\}\alpha + \mathcal{E}_0\mathcal{T}e^{-i\phi_0},$$
$$\dot{\beta}_j = -\left(i\Omega_j + \frac{\Gamma_j}{2}\right)\beta_j + ig_j|\alpha|^2. \quad (3)$$

In addition to dispersive optomechanical coupling, the cavity absorbs photons and heats up, which in turn changes its refractive index and geometry. We model this process through the dynamics of the temperature deviation $\delta\dot{T}(t) = g_{\mathrm{abs}}|\alpha|^2(t) - \gamma_{\mathrm{th}}\delta T(t)/2$, and the resulting shift of the optical frequency $\omega_{\mathrm{op}} \approx \omega_{\mathrm{op}}(\bar{T}) + (\partial\omega_{\mathrm{op}}/\partial T)\times[T(t) - \bar{T}] = \omega_0 + g_T\delta T(t)$. Here, g_{abs} denotes the temperature change due to linear photon absorption, γ_{th} the thermalization rate, and g_T the linearized thermo-optical frequency shift [44–48]. The mean mechanical fields $\beta_j(t)$ and temperature deviation $\delta T(t)$ are expressible via the mean intensity $|\tilde{\alpha}|^2(\omega)$ in Fourier space. Since the equation for the mean optical field α is temporally periodic, we choose a Floquet ansatz and express α as a truncated Fourier series $\alpha(t) = \sum_n \alpha_n e^{-in\Omega_{\mathrm{mod}}t}$ with $n \in \{-D, \ldots, D\}$. The resulting mean field intensity is then $|\tilde{\alpha}|^2(\omega) = \sum_{(p,q)}\alpha_p\alpha^*_{p-q}\delta(\omega - iq\Omega_{\mathrm{mod}})$, where $p \in \{-D, \ldots, D\}$ and $q \in \{-D + p, \ldots, D + p\}$. The Floquet ansatz results in the dynamics of the optical mean field

$$\dot{\alpha}_m = \mathcal{E}_0\mathcal{T}_m - \chi_m^{-1}\alpha_m + \sum_{(p,q)}\chi^{-1}_{\mathrm{cub},q}\alpha_p\alpha^*_{p-q}\alpha_{m-q}. \quad (4)$$

Acquiring its steady state ($\dot{\alpha}_m = 0$) amounts to solving $4D + 2$ coupled real cubic equations, applicable to other Kerr-like models [50–52]. Here, we defined $\mathcal{T}_0 = [1 - i\mathcal{J}_0(d)]/2$, $\mathcal{T}_m = i^{|m|+1}\mathcal{J}_m(d)$, $\chi_m^{-1} = i(\Delta - m\Omega_{\mathrm{mod}}) + \kappa/2$, and $\chi^{-1}_{\mathrm{cub},q} = \chi^{-1}_{\mathrm{Th},q} + \sum_j \chi^{-1}_{\mathrm{OM},jq}$ with $2\pi\chi^{-1}_{\mathrm{Th},q}/g_T g_{\mathrm{abs}} = (q\Omega_{\mathrm{mod}} - i\gamma_{\mathrm{th}}/2)^{-1}$ and $2\pi\chi^{-1}_{\mathrm{OM},jq}/g_j^2 = [i(q\Omega_{\mathrm{mod}} - \Omega_j) - \Gamma_j/2]^{-1} - [i(q\Omega_{\mathrm{mod}} + \Omega_j) + \Gamma_j/2]^{-1}$. The steady state $\bar{\alpha}_m$ is attainable analytically [53] for $D = 0$ and numerically otherwise.

The resulting $\bar{\alpha}_m$ turn the dynamics of fluctuation components $\hat{\mathfrak{a}}$ and $\hat{\mathfrak{b}}$ into a periodic system treatable with Floquet techniques [37] up to leading order,

$$\dot{\hat{\mathfrak{a}}}^{(0)} = \tilde{\chi}^{-1}\hat{\mathfrak{a}}^{(0)} + \sum_n\sum_{j=1}^{N} ig_j\bar{\alpha}_n\mathfrak{R}(\hat{\mathfrak{b}}_j^{(n)}) + \sqrt{\kappa}\hat{\mathfrak{a}}^{(0)}_{\mathrm{in}},$$
$$\dot{\hat{\mathfrak{b}}}_j^{(n)} = \check{\chi}_{jn}^{-1}\hat{\mathfrak{b}}_j^{(n)} + ig_j[\bar{\alpha}^*_{-n}\hat{\mathfrak{a}}^{(0)} + \bar{\alpha}_n\hat{\mathfrak{a}}^{\dagger(0)}] + \sqrt{\Gamma_j}\hat{\mathfrak{b}}^{(n)}_{j,\mathrm{in}}, \quad (5)$$

with the mechanical Floquet susceptibilities $\check{\chi}_{jn}^{-1} = -[i(\Omega_j - n\Omega_{\mathrm{mod}}) + \Gamma_j/2]$ and the optical susceptibility $\tilde{\chi}^{-1} = -[i(\Delta - \sum_j g_j^2|\bar{\alpha}_0|^2 I(\check{\chi}_{j0}^{-1})/|\check{\chi}_{j0}^{-1}|^2) + \kappa/2]$ where we denote $\mathfrak{R}(\hat{o}) = \hat{o} + \hat{o}^\dagger$ and $I(z) = i(z^* - z)$. Using the input-output relations for the relevant optical output field $\hat{\mathfrak{a}}_{\mathrm{out}}(\omega) = \hat{\mathfrak{a}}^{(0)}_{\mathrm{in}}(\omega) - \sqrt{\kappa}\hat{\mathfrak{a}}^{(0)}(\omega)$ and input noise obeying $\langle\hat{\mathfrak{u}}^{(m)}_{\mathrm{in}}(\omega)\hat{\mathfrak{w}}^{\dagger(p)}_{\mathrm{in}}(\omega')\rangle = \delta(\omega - \omega')\delta_{\mathfrak{u}\mathfrak{w}}\delta_{mp}(\mathfrak{n}^{\mathfrak{u}}_{\mathrm{th}} + 1)$ characterized by the average thermal occupations $\mathfrak{n}^{\mathfrak{u}}_{\mathrm{th}}$ yields the stationary power spectral density of the optical output field

$$S_{\mathrm{op}}(\omega) = \tilde{S} + \sum_{n,j}\frac{\kappa g_j^2|\bar{\alpha}_n|^2\Gamma_j\mathfrak{n}^{\mathfrak{b}_j}_{\mathrm{th}}}{[(\omega - \bar{\Delta})^2 + \frac{\kappa^2}{4}][(\omega - \Omega_{jn})^2 + \frac{\Gamma_j^2}{4}]}. \quad (6)$$

This quantity is experimentally accessible in a direct measurement and consisting of a noise floor $\tilde{S}$ and multiple Lorentzian peaks at $\Omega_{jn} = \Omega_j + n\Omega_{\mathrm{mod}}$. In sideband unresolved systems ($\kappa \gg \Omega_{jn}$), these are filtered equally by the Lorentzian cavity density of states with effective detuning $\bar{\Delta} = \Delta + \sum_{j,n} 2g_j^2|\bar{\alpha}_n|^2/\Omega_j$, due to static radiation pressure for $\Gamma_j \ll \Omega_j$. Consequently, the spectrum displays the mean field amplitudes $|\bar{\alpha}_n|^2$ in leading order.

Results with one mechanical mode.—Aiming to observe the model dynamics with one mechanical mode, we use a 265 nm thin InP 10×20 μm^2 membrane suspended over a rib silicon waveguide via a 250 nm air-gap illustrated in Fig. 1(a). The membrane is pierced with a 2D photonic crystal and two L3 defect cavities at its center. These defects, shown in the inset of Fig. 1(a), allow localized photonic modes to be evanescently driven from the waveguide. The optical channel transmission spectrum is measured by injecting a broadband light source into the

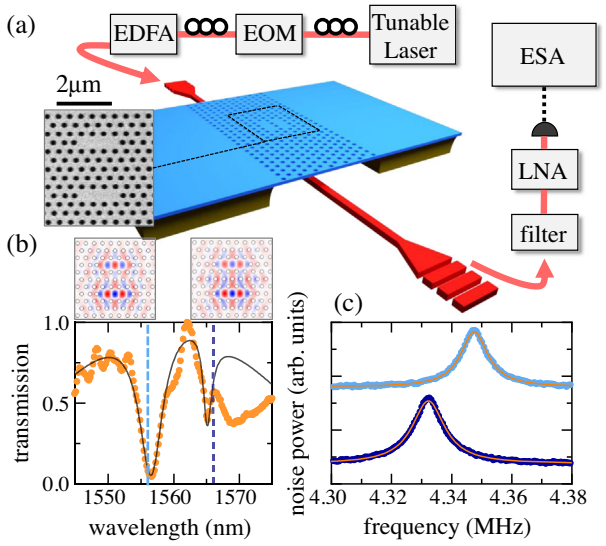

FIG. 1. (a) Experimental setup including the integrated optomechanical platform with a suspended 2D photonic crystal InP nanomembrane (blue) above a SOI waveguide (red). Inset: SEM micrograph of the L3 defects. (b) Measured transmission spectrum (orange dots) and fit (black line). The electric field distribution associated with each photonic resonance are shown on top. (c) Mechanical spectrum measured by optomechanically probing the photonic mode (−) (dark blue) or the mode (+) (light blue). The photothermal effect induces different elastic property changes resulting in different frequencies.

waveguide gratings termination. The transmitted field is collected and sent to a monochromator. The normalized transmission spectrum is plotted in Fig. 1(b). We fit the data using the coupled mode theory (CMT) of two waveguide-coupled photonic cavities [54] and ignore the right most feature. The bonding and antibonding modes central wavelengths are fitted as $\lambda_- = 1557.27$ nm and $\lambda_+ = 1565.55$ nm, with total quality factors $Q_-^{\mathrm{tot}} \approx 380$ and $Q_+^{\mathrm{tot}} \approx 3240$. The discrepancy between fit and data around 1570 nm results from imperfect alignment of the injection and collection fiber tips with regard to the SOI gratings. The simulated distributions of the transverse electric field component for both modes are shown in Fig. 1(b). We perform all measurements at room temperature with the chip placed in a vacuum chamber pumped below 10^{-5} mbar.

To access the mechanical noise spectrum of the suspended membrane, a tunable laser resonantly drives a given optical mode [dashed vertical lines in Fig. 1(b)]. The output signal is filtered, sent to a low noise amplifier (LNA), and coupled to a low-sensitivity photodetector. We measure the resulting rf signal with an electrical spectrum analyzer (ESA). The suspended membrane sustains several mechanical modes with frequencies ranging from 4 MHz to more than 100 MHz. These resonances interact with the optical modes through dissipative and dispersive optomechanical couplings [55]. As illustrated in Fig. 1(c), the mechanical spectrum can be accessed by driving either the bonding (light blue) or antibonding (dark blue) optical mode. In this work we focus on the fundamental mechanical mode with central frequency $\Omega_1 = 2\pi \times 4.330$ MHz and linewidth $\Gamma_1 = 2\pi \times 6$ kHz.

Before injecting into the system, the laser with wavelength $\lambda_L = 1565.75$ nm passes a MZM subjected to an rf signal $V(t) = V_{\mathrm{mod}} \cos \Omega_{\mathrm{mod}} t$. The modulation depth is $d = \pi \times V_{\mathrm{mod}}/V_\pi$ with the calibrated half-wave voltage $V_\pi = 7.0$ V. We record the output optical field noise spectrum as illustrated in Fig. 2(a). The resulting experimental diagrams using a modulation depth of $d = 0.89$ are depicted in Fig. 2(b). The top figure shows the result for the input power $P_{\mathrm{in}} = 1.3$ mW which yields a thermo-optic bistability (see Supplemental Material [56]). At this input power and wavelength λ_L, the probing laser is put centrally in this bistable regime. We observe modulation sidebands surrounding the mechanical peak, with imbalanced amplitudes because of thermo-optical effects. For comparison, the identical measurement realized in the low-power situation is shown in the bottom of Fig. 2(b). In this case, only one pair of sidebands with weak and balanced amplitudes are recorded. Neglecting higher order contributions (see Supplemental Material [56]), the numerical prediction by Eq. (6) with $\Omega_1 = 2\pi \times 4.34$ MHz, $g_1/\Omega_1 = 2.30 \times 10^{-2}$, $\Gamma_1/\Omega_1 = 7.35 \times 10^{-2}$, $\kappa/\Omega_1 = 1.36 \times 10^4$, $\Delta/\Omega_1 = 1.65 \times 10^4$ is presented in the top of Fig. 2(c) showing qualitative agreement with the experiment at large input power. We employ a drive of $\mathcal{E}_0/\Omega_1 = 4.62 \times 10^4$ and modulation depth $d = 1.35$ in addition with the thermo-optical coupling strength $g_T g_{\mathrm{abs}}/g_1^2 = 2.54 \times 10^2$ and thermalization rate $\gamma_{\mathrm{th}} = 2\pi \times 112$ kHz. These parameters amount to a blueshift ($g_T g_{\mathrm{abs}}/\gamma_{\mathrm{th}} > 0$) for temperature fluctuations previously found in silicon [44]. This can be attributed to changes in the cavity's elastic properties [57] and geometry rather than a change in the refractive index. We find that Ω_{mod} allows control over the transduced modulation comb. This effect requires sufficiently high input power and modulation frequencies below 125 kHz. This cut-off frequency originates from the thermalization rate of the material. In an independent measurement (see Supplemental Material [56]), we measure the switching transition time of approximately 4 μs in the thermo-optic resonator, in good agreement with previous measurements in a similar device [58]. Higher modulation frequency suppresses the thermo-optic effect but maintains the amount of visible sidebands (in contrast to the heterodyne measurement in [44]). Consequently, the modulation comb retains its symmetry. We perform a measurement as a function of the modulation depth (see Supplemental Material [56]) and find that this parameter also enables control over the modulation comb asymmetry. Numerical simulations of Eq. (6) with a reduced driving strength $\mathcal{E}_0/g_1 = 10^3$ and modulation depth $d = 0.89$ shown in the bottom of Fig. 2(c) agree with the experimental result and show only one pair of symmetric sidebands. Horizontal

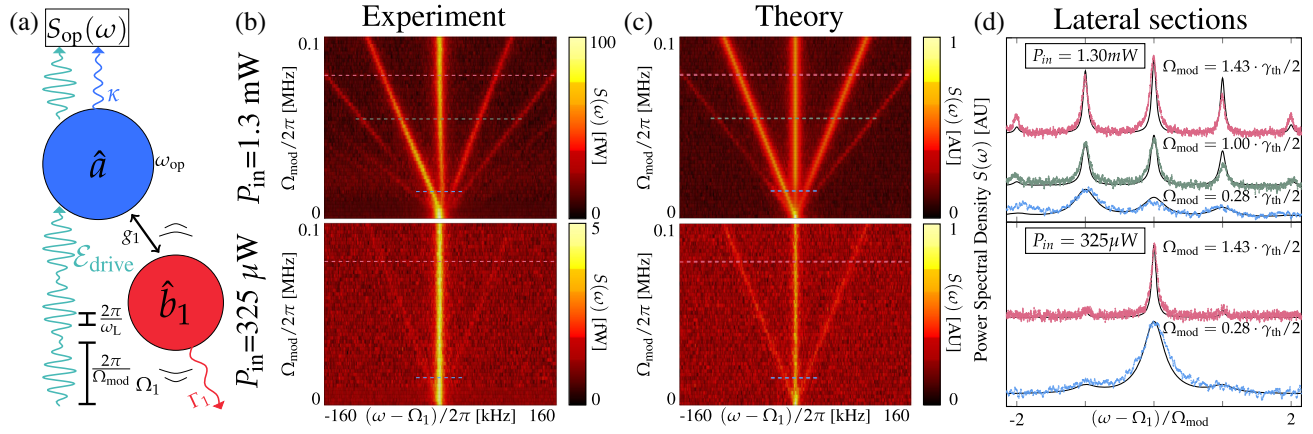

FIG. 2. Floquet dynamics of a single-mode optomechanical system (a) Schematic of an optomechanical cavity driven with a modulated laser field. (b) Experimentally measured noise spectra centered at the mechanical frequency $\Omega_1 = 2\pi \times 4.330$ MHz for $P_{\rm in} = 1.3$ mW (top) and $P_{\rm in} = 325$ μW (bottom) mapped over the modulation frequency $\Omega_{\rm mod}$. (c) Theoretically predicted noise spectra for varying $\Omega_{\rm mod}$ employing high (top) and low (bottom) optical power. (d) Lateral sections along the dotted lines in (b) and (c) of the measured spectra (dotted) and numerical results (solid).

sections of the respective theoretical (solid) and experimental (dotted) heat maps are shown in Fig. 2(d) for large (top) and low (bottom) input power for $\Omega_{\rm mod} = 0.28 \times \gamma_{\rm th}/2$ (blue), $\Omega_{\rm mod} = 1.00 \times \gamma_{\rm th}/2$ (green), and $\Omega_{\rm mod} = 1.43 \times \gamma_{\rm th}/2$ (red) demonstrating the thermal decay rate $\gamma_{\rm th}/2$ to define the cut-off frequency and confirming the observed model dynamics.

Floquet control of optomechanical bistability.—Based on our model and its agreement with experiment for one mechanical mode, we extend the discussion to potential applications with multimode systems. We can analyze the interaction of the mechanical Floquet modes $\hat{\mathfrak{b}}_j^{(m)}$ mediated through the optical field fluctuations by eliminating $\hat{\mathfrak{a}}^{(0)}$ and find their effective coupling via the contributions

$$\sigma_{jlp}^{(m)}(\omega) = \frac{g_j g_l \bar{\alpha}_{-m}^* \bar{\alpha}_p}{i(\bar{\Delta}-\omega)+\frac{\kappa}{2}} - \frac{g_j g_l \bar{\alpha}_m \bar{\alpha}_p^*}{-i(\bar{\Delta}+\omega)+\frac{\kappa}{2}}. \tag{7}$$

The stationary mechanical spectra without periodic drive ($m \equiv p \equiv 0$) are Lorentzians [34,59] $S_{\hat{\mathfrak{b}}_j}(\omega) = \tilde{S}_{\hat{\mathfrak{b}}_j} + \Gamma_j \bar{n}_j [(\Omega_j' - \omega)^2 + \Gamma_j'^2/4]^{-1}$ with optical-spring-corrected frequencies $\Omega_j' = \Omega_j \sqrt{I[\sigma_{jj0}^{(0)}(\Omega_j)]/(4\Omega_j) + 1}$ and modified linewidths $\Gamma_j' = \Gamma_j + R[\sigma_{jj0}^{(0)}(\Omega_j)]$. Such expressions allow assessing optomechanical and photothermal [60] backaction as negligible in our system (see Supplemental Material [56]). Moreover, the former expression contains information about the stability of mechanical oscillators' steady states for red-detuned driving ($\bar{\Delta} > 0$): if we examine the static frequency response we find $\Omega_j'(\omega=0) = \Omega_j \sqrt{\eta_j}$ with $\eta_j = 1 - \bar{\Delta} g_j^2 |\bar{\alpha}_0|^2 / [\Omega_j(\bar{\Delta}^2 + \kappa^2/4)]$ which has to be larger than zero for a stable steady state according to the Routh-Hurwitz criterion [34]. In the presence of the periodic drive, there are additional contributions to the frequency response which modify the stability parameter

$$\tilde{\eta}_j = \eta_j + \frac{1}{4\Omega_j} \sum_{n,l\neq j} I\left[\frac{\sigma_{jln}^{(0)} \sigma_{jl0}^{(n)}}{i(\Omega_l - n\Omega_{\rm mod}) + \frac{\Gamma_l}{2} + \sigma_{jln}^{(n)}}\right]. \tag{8}$$

This suggests that a mechanical mode $\hat{b}_l$ can influence the occurrence of the optomechanical bistability of a distinct mechanical mode $\hat{b}_j$ if the modulation frequency is tuned into resonance at $\Omega_{\rm mod} = \Omega_l/n$ with $n \in \mathbb{Z}$ on the scale of the mechanical linewidth Γ_l. We investigate the predicted capability of the periodic drive in Eq. (8) to control the bistability of a distinct mechanical mode as depicted in Fig. 3(a). We therefore conduct numerical simulations with system parameters which exhibit an optomechanical bistability based on [26]. It consists of a mechanical oscillator with frequency $\Omega_1 = 2\pi \times 10$ MHz, damping rate $\Gamma_1/\Omega_1 = 5.00 \times 10^{-2}$, coupled with the rate $g_1/\Omega_1 = 1.52 \times 10^{-5}$ to an optical field with decay rate $\kappa/\Omega_1 = 1.40$, detuning $\Delta/\Omega_1 = 2.62$, and $\mathcal{E}_0/\Omega_1 = 1.44 \times 10^5$. Additionally, a second mechanical mode with frequency $\Omega_2/\Omega_1 = 1.10$, damping rate $\Gamma_2/\Omega_1 = 5.50 \times 10^{-3}$, and coupling strength $g_2/g_1 = 5.53 \times 10^{-2}$ is used to control the prior one's steady state. We omit the thermo-optical effect ($g_T = 0$) and inspect the effect of intensity modulation with modulation depth $d = 1.875 \times 10^{-5}$ on the mean field dynamics of the Itô stochastic differential equation corresponding to Eq. (3). We study thermal excitation corresponding to shot noise $n_{\rm th}^{\mathfrak{a}} = n_{\rm th}^{\mathfrak{b}_1} = 0$ for the cavity and the bistable mechanical mode and $n_{\rm th}^{\mathfrak{b}_2} = 8000$ phonons employing the Euler-Maruyama scheme [61]. This setting makes the system experience noise

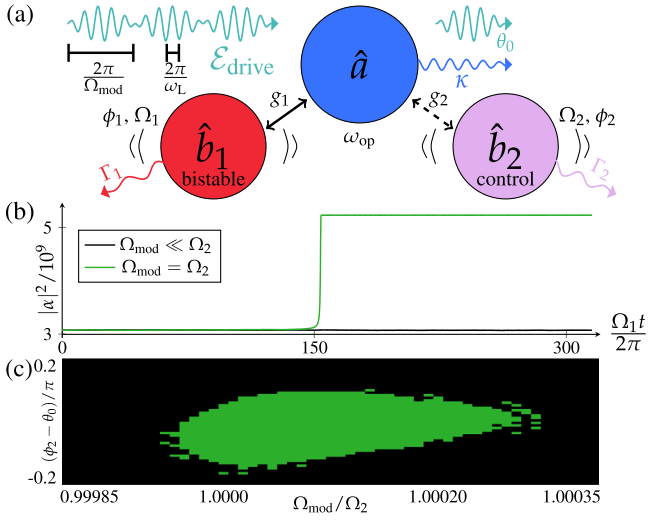

FIG. 3. Floquet control of optomechanical bistability. (a) An optomechanically bistable mode is controlled by another nondegenerate control mode with an intensity-modulated pump. (b) The steady state switches when the modulation frequency Ω_{mod} matches the control frequency Ω_2 (green) whereas it is unaffected for off-resonant modulation (black). (c) Two-dimensional parameter diagram describing the switching capability of the Floquet drive: the intensity modulation's phase θ_0 aligning with the mechanical phase ϕ_2 in addition to the frequency matching leads to steady state switching (green).

predominantly in the control mode $\hat{b}_2$. Its mean field displacement $R(\beta_2) = \bar{q}_2 \cos[\Omega_2 t + \phi_2(t)]$ will therefore encounter phase noise $\phi_2(t)$ described by a Wiener process. The examples in Fig. 3(b) show that the system remains stable in its steady state for off-resonant modulation $\Omega_{\mathrm{mod}} = 2\pi \times 1$ MHz $\ll \Omega_2$. For sufficient time under resonant modulation $\Omega_{\mathrm{mod}} = \Omega_2$, switching of the steady state occurs (see Supplemental Material [56]) and enables the setup to detect a signal at frequency Ω_2 in the signal fed into the MZM. Figure 3(c) summarizes the result of omitting thermal excitation and replacing it with periodic drive to clarify the switching mechanism: switching of the steady state occurs if the now deterministic phase ϕ_2 of the mechanical oscillator used to control the bistability aligns with the phase θ_0 of the optical modulation for resonant intensity modulation. This requires the control oscillator to assume the correct phase for sufficiently long optical modulation (see Supplemental Material [56]). Thermal excitation causes phase noise and will eventually ensure the phase-sensitive switching. Tuning the modulation depth, we find that the amplitude of the sidebands $\bar{\alpha}_n$ can be increased or reduced for modulation frequencies in the thermo-optical regime (see Supplemental Material [56]). Since Eq. (8) suggests that the underlying coupling strength grows (nonlinearly) with these amplitudes, photothermal effects and thermal excitation can be exploited for increased control of multimode optomechanical systems.

Conclusions.—Our investigation reveals that thermal properties of optomechanical systems can be employed to tailor its Floquet dynamics. Using a 2D sideband unresolved optomechanical photonic crystal, we demonstrated experimentally how a Kerr-type nonlinearity—namely the thermo-optic effect—can achieve the predicted desymmetrization. This method conveniently characterizes thermal properties which we verify with independent measurements. Interestingly such nonlinearities are ubiquitous in semiconductor microcavities, with cut-off frequencies ranging from a few kilohertz and surpassing the GHz range [62], depending on the process nature. These Floquet modes allow us to control the bistability of a distinct mechanical mode which can be understood from higher-order cross-mode contributions to the self-energy with modulated drive. We demonstrated the operation of this mechanism with two mechanical modes where the thermal excitation of one mode allows resonant modulation to trigger a response of the other. This mechanism applies equally to multiple harmonically spaced control modes where the switching can implement logical rules.

This work is supported by the European Union's Horizon 2020 research and innovation program under Grant Agreement No. 732894 (FET Proactive HOT), the Julian Schwinger Foundation project Grant No. JSF-16-03-0000 (TOM), the French RENATECH network, the Agence Nationale de la Recherche as part of the "Investissements d'Avenir" program (Labex NanoSaclay, ANR-10-LABX-0035) with the flagship project CONDOR and the JCJC project ADOR (ANR-19-CE24-0011-01).

*karl.a.pelka@um.edu.mt
†guilhem.madiot@icn2.cat

[1] M. Aspelmeyer, T. J. Kippenberg, and F. Marquardt, Rev. Mod. Phys. **86**, 1391 (2014).
[2] T. J. Kippenberg, H. Rokhsari, T. Carmon, A. Scherer, and K. J. Vahala, Phys. Rev. Lett. **95**, 033901 (2005).
[3] F. Marquardt, J. G. E. Harris, and S. M. Girvin, Phys. Rev. Lett. **96**, 103901 (2006).
[4] J. D. Teufel, T. Donner, D. Li, J. W. Harlow, M. S. Allman, K. Cicak, A. J. Sirois, J. D. Whittaker, K. W. Lehnert, and R. W. Simmonds, Nature (London) **475**, 359 (2011).
[5] J. Chan, T. P. M. Alegre, A. H. Safavi-Naeini, J. T. Hill, A. Krause, S. Gröblacher, M. Aspelmeyer, and O. Painter, Nature (London) **478**, 89 (2011).
[6] C. F. Ockeloen-Korppi, E. Damskägg, J. M. Pirkkalainen, M. Asjad, A. A. Clerk, F. Massel, M. J. Wooley, and M. A. Sillanpää, Nature (London) **556**, 478 (2018).
[7] R. Riedinger, A. Wallucks, I. Marinković, C. Löschnauer, M. Aspelmeyer, S. Hong, and S. Gröblacher, Nature (London) **556**, 473 (2018).
[8] G. Heinrich, M. Ludwig, J. Qian, B. Kubala, and F. Marquardt, Phys. Rev. Lett. **107**, 043603 (2011).
[9] R. Lauter, C. Brendel, S. J. M. Habraken, and F. Marquardt, Phys. Rev. E **92**, 012902 (2015).

[10] R. Lauter, A. Mitra, and F. Marquardt, Phys. Rev. E **96**, 012220 (2017).
[11] C. A. Holmes, C. P. Meaney, and G. J. Milburn, Phys. Rev. E **85**, 066203 (2012).
[12] N. Lörch, S. E. Nigg, A. Nunnenkamp, R. P. Tiwari, and C. Bruder, Phys. Rev. Lett. **118**, 243602 (2017).
[13] E. Amitai, N. Lörch, A. Nunnenkamp, S. Walter, and C. Bruder, Phys. Rev. A **95**, 053858 (2017).
[14] M. Zhang, G. S. Wiederhecker, S. Manipatruni, A. Barnard, P. McEuen, and M. Lipson, Phys. Rev. Lett. **109**, 233906 (2012).
[15] M. Zhang, S. Shah, J. Cardenas, and M. Lipson, Phys. Rev. Lett. **115**, 163902 (2015).
[16] M. F. Colombano, G. Arregui, N. E. Capuj, A. Pitanti, J. Maire, A. Griol, B. Garrido, A. Martínez, C. M. Sotomayor-Torres, and D. Navarro-Urrios, Phys. Rev. Lett. **123**, 017402 (2019).
[17] K. Pelka, V. Peano, and A. Xuereb, Phys. Rev. Research **2**, 013201 (2020).
[18] G. Madiot, F. Correia, S. Barbay, and R. Braive, Phys. Rev. A **104**, 023525 (2021).
[19] P. E. Allain, B. Guha, C. Baker, D. Parrain, A. Lemaître, G. Leo, and I. Favero, Phys. Rev. Lett. **126**, 243901 (2021).
[20] N. R. Bernier, L. D. Tóth, A. Koottandavida, M. A. Ioannu, D. Malz, A. Nunnenkamp, A. K. Feofanov, and T. J. Kippenberg, Nat. Commun. **8**, 604 (2017).
[21] D. Malz, L. D. Tóth, N. R. Bernier, A. K. Feofanov, T. J. Kippenberg, and A. Nunnenkamp, Phys. Rev. Lett. **120**, 023601 (2018).
[22] S. Barzanjeh, M. Wulf, M. Peruzzo, M. Kalaee, P. B. Dieterle, O. Painter, and J. M. Fink, Nat. Commun. **8**, 953 (2017).
[23] L. Mercier de Lépinay, E. Damskägg, C. F. Ockeloen-Korppi, and M. A. Sillanpää, Phys. Rev. Applied **11**, 034027 (2019).
[24] R. W. Andrews, R. W. Peterson, T. P. Purdy, K. Cicak, R. W. Simmonds, C. A. Regal, and K. W. Lehnert, Nat. Phys. **10**, 321 (2014).
[25] A. Dorsel, J. D. McCullen, P. Meystre, E. Vignes, and H. Walther, Phys. Rev. Lett. **51**, 1550 (1983).
[26] R. Ghobadi, A. R. Bahrampour, and C. Simon, Phys. Rev. A **84**, 033846 (2011).
[27] M. Bagheri, M. Poot, M. Li, W. P. H. Pernice, and H. X. Tang, Nat. Nanotechnol. **6**, 726 (2011).
[28] H. Xu, U. Kemiktarak, J. Fan, S. Ragole, J. Lawall, and J. M. Taylor, Nat. Commun. **8**, 14481 (2017).
[29] R. L. Badzey, G. Zolfagharkhani, A. Gaidarzhy, and P. Mohanty, Appl. Phys. Lett. **85**, 3587 (2004).
[30] I. Maboob and H. Yamaguchi, Nat. Nanotechnol. **3**, 275 (2008).
[31] S. O. Erbil, U. Hatipoglu, C. Yanik, M. Ghavami, A. B. Ari, M. Yuksel, and M. S. Hanay, Phys. Rev. Lett. **124**, 046101 (2020).
[32] S. R. K. Rodriguez, W. Casteels, F. Storme, N. Carlon Zambon, I. Sagnes, L. Le Gratiet, E. Galopin, A. Lemaître, A. Amo, C. Ciuti, and J. Bloch, Phys. Rev. Lett. **118**, 247402 (2017).
[33] T. Fink, A. Schade, S. Höfling, C. Schneider, and A. Imamoglu, Nat. Phys. **14**, 365 (2018).
[34] C. Genes, A. Mari, D. Vitali, and P. Tombesi, Adv. At. Mol. Opt. Phys. **57**, 33 (2009).
[35] M. Rossi, N. Kralj, S. Zippilli, R. Natali, A. Borrielli, G. Pandraud, E. Serra, G. Di Giuseppe, and D. Vitali, Phys. Rev. Lett. **120**, 073601 (2018).
[36] A. Mari and J. Eisert, Phys. Rev. Lett. **103**, 213603 (2009).
[37] D. Malz and A. Nunnenkamp, Phys. Rev. A **94**, 023803 (2016).
[38] I. Pietikäinen, O. Černotik, and R. Filip, New J. Phys. **22**, 063019 (2020).
[39] H. Xu, L. Jiang, A. A. Clerk, and J. G. E. Harris, Nature (London) **568**, 65 (2019).
[40] V. Peano, C. Brendel, M. Schmidt, and F. Marquardt, Phys. Rev. X **5**, 031011 (2015).
[41] S. Walter and F. Marquardt, New J. Phys. **18**, 113029 (2016).
[42] J. P. Mathew, J. del Pino, and E. Verhagen, Nat. Nanotechnol. **15**, 198 (2020).
[43] M. J. Weaver, F. Buters, F. Luna, H. Eerkens, K. Heeck, S. de Man, and D. Bouwmeester, Nat. Commun. **8**, 824 (2017).
[44] L. Qiu, I. Shomroni, M. A. Ioannou, N. Piro, D. Malz, A. Nunnenkamp, and T. J. Kippenberg, Phys. Rev. A **100**, 053852 (2019).
[45] M. Eichenfield, R. Camacho, J. Chan, K. J. Vahala, and O. Painter, Nature (London) **459**, 550 (2009).
[46] E. Verhagen, S. Deléglise, S. Weis, A. Schliesser, and T. J. Kippenberg, Nature (London) **482**, 63 (2012).
[47] J. Li, S. Diddams, and K. J. Vahala, Opt. Express **22**, 14559 (2014).
[48] J. Ma, G. Guccione, R. Lecamwasam, J. Qin, G. T. Campbell, B. C. Buchler, and P. K. Lam, Optica **8**, 177 (2021).
[49] L. Mercadé, K. Pelka, R. Burgwal, A. Xuereb, A. Martínez, and E. Verhagen, Phys. Rev. Lett. **127**, 073601 (2021).
[50] R. Garcés and G. J. de Valcárel, Sci. Rep. **6**, 21964 (2016).
[51] M. A. Castellanos-Beltran, K. D. Irwin, G. C. Hilton, L. R. Vale, and K. W. Lehnert, Nat. Phys. **4**, 929 (2008).
[52] G. Kirchmair, B. Vlastakis, Z. Leghtas, S. E. Nigg, H. Paik, E. Ginossar, M. Mirrahimi, L. Frunzio, S. M. Girvin, and R. J. Schoelkopf, Nature (London) **495**, 205 (2013).
[53] B. Hassett, *Introduction into Algebraic Geometry* (Cambridge University Press, Cambridge, England, 2007).
[54] Q. Li, T. Wang, Y. Su, M. Yan, and M. Qiu, Opt. Express **18**, 8367 (2010).
[55] V. Tsvirkun, A. Surrente, F. Raineri, G. Beaudoin, R. Raj, I. Sagnes, I. Robert-Philip, and R. Braive, Sci. Rep. **5**, 16526 (2015).
[56] See Supplemental Material at http://link.aps.org/supplemental/10.1103/PhysRevLett.129.123603 for the experimental characterisation of the thermal bistability and its parameters; an assessment of dynamical backaction effects; an outline of the numerical algorithm displaying the bistability control; and the influence of modulation depths on the control.

[57] P. S. Branicio, J. P. Rino, C. K. Gan, and H. Tsuzuki, J. Phys. Condens. Matter **21**, 095002 (2009).

[58] M. Brunstein, R. Braive, R. Hostein, A. Beveratos, I. Robert-Philip, I. Sagnes, T. J. Karle, A. M. Yacomotti, J. A. Levenson, V. Moreau, G. Tessier, and Y. De Wilde, Opt. Express **17**, 17118 (2009).

[59] M. Karuza, C. Molinelli, M. Galassi, C. Biancofiore, R. Natali, P. Tombesi, G. Di Giuseppe, and D. Vitali, New J. Phys. **14**, 095015 (2012).

[60] J. Restrepo, J. Gabelli, C. Ciuti, and I. Favero, C.R. Phys. **12**, 860 (2011).

[61] P. E. Kloeden and E. Platen, *Numerical Solution of Stochastic Differential Equations* (Springer-Verlag, Berlin-Heidelberg, 1992).

[62] J. S. Pelc, K. Rivoire, S. Vo, C. Santori, D. A. Fattal, and R. G. Beausoleil, Opt. Express **22**, 3797 (2014).